Secondary-electron-production cross sections for electron-impact ionization of molecular nitrogen

R. R. Goruganthu, W. G. Wilson, and R. A. Bonham
Department of Chemistry, Indiana University, Bloomington, Indiana 47405
(Received 28 April 1986)

Measurements of the double-differential cross section (DDCS), as a function of the ejected energy, angle, and primary energy for electron-impact ionization of molecular nitrogen are reported at incident energies of 200, 500, 1000, and 2000 eV. The ejection angle was varied from 30° to 150° in steps of 15°. The cross sections were obtained by use of a crossed-beam apparatus with an effusive gas source and a pulsed electron beam. Scattered and ejected electrons were energy analyzed by time-of-flight analysis from below 2 eV to the primary energy. The relative measurements were placed on an absolute scale by matching the experimental elastic differential cross sections to absolute measurements at each primary energy. Comparisons of the DDCS with previous reported values revealed significant differences. The DDCS were fitted to a Legendre polynomial expansion as a function of the ejection angle. Platzman plot analysis was carried out on the energy distributions determined from the fit coefficients. The total ionization cross sections at these primary energies were deduced from this plot. An autoionization feature at 2.3 eV was observed for the first time in measurements of this nature and has been assigned as due to a Rydberg state converging to the $B\,^2\Sigma_u^+$ ionic state which decays to the $X\,^2\Sigma_g^+$ ground state of N_2^+. An analysis of the autoionization lines observed in the present work in the range 0.4—2.5 eV is also presented.

I. INTRODUCTION

In an earlier paper[1] we presented the cross-section differential in ejected energy and angle for electron-impact ionization of helium in the primary electron energy range of 200—2000 eV. Since nitrogen is the most abundant atmospheric gas, measurements of differential ionization cross sections are of particular interest and have been studied extensively[2–7] in the past two decades. In light of the disagreements in the shape of the angular distributions of ejected electrons from molecular nitrogen among the previously reported measurements, it is necessary to undertake a remeasurement with better accuracy.

The earliest measurements of the double-differential cross section (DDCS), $d^2\sigma/dWd\Omega$, as a function of the ejected energy W, angle θ, and primary energy T, for N_2 were made by Mohr and Nicoll[2] in 1934 in the primary energy range 20—300 eV and the angular range of 15° to 155°. Since then there have not been any reported measurements of these quantities until those of Opal, Beaty, and Peterson[3] (OBP) in 1972. Their primary energies were from 50 to 2000 eV and covered the angular range 30° to 150°. Problems with their angular distributions at very small and very large angles have been pointed out by a number of authors.[4–6] DuBois and Rudd[4] have measured the DDCS in the angular range of 10° to 150° for 100—500-eV primary electrons using a static gas cell. These authors have pointed out reasons for the discrepancy between their angular distributions of the DDCS and those of OBP. The angular resolution in the OBP experiment was 10° and they considered their gas beam source to be uncollimated. Based on these factors DuBois and Rudd have suggested a correction factor of the type $a+(1-a)\sin\theta$ with $a=0.10$. Unfortunately the experiment of DuBois and Rudd suffered from spurious structure in the forward angles and transmission problems for low-energy (<10 eV) secondary electrons.[6] Oda[7] has reported the DDCS for 500-eV primary electrons and later Oda, Nishimura, and Ossawa[6] have reported measurements covering the primary energy range 100—1000 eV and ejection angles from 5° to 140°. Their lowest ejected energy was 10 eV.

Kim[8–10] has pointed out that the single-differential and the total ionization cross sections are extremely useful in understanding the systematics of the ionization process. Most previous measurements are deficient in that the DDCS data for ejected electrons with low energies, which contribute significantly to the total ionization cross section, were not measured. However, Shyn[11] has reported measurements of the DDCS for ejected energies W down to 1 eV for primary electron energies T from 50 to 400 eV in the angular range of 12° to 156°. This experiment employed a crossed-beam method. As in a previous experiment on the measurement of the DDCS for helium[12] their results exhibited a peak for low-energy ejected electrons in the forward direction similar to that reported by DuBois and Rudd.[4]

None of the measurements reported since OBP (Ref. 3) have covered a wide enough range of primary energies to make systematic checks[8–10] and hence are not optimal for use in applications related to radiation chemistry, biology, or plasma physics.[13] In this paper we present measurements of the DDCS for primary electrons of energy 200, 500, 1000, and 2000 eV in the angular range 30°—150° using a crossed-beam apparatus with time-of-flight energy analysis for scattered and ejected electrons together with systematic checks on the measured cross sections.

II. EXPERIMENTAL METHOD

The details of the apparatus were given in an earlier publication.[1] A schematic of the apparatus used is given in Fig. 1. The apparatus consisted of a pulsed electron beam obtained by sweeping an electron beam produced from a commercially available electron gun across a skimmer with an aperture 1 mm in diameter. The electron pulse intersects at a right angle an effusive gas beam produced by passing gas through a hypodermic needle. The scattering angle was variable from 30° to 150° by using the second drift region shown in Fig. 1. The first drift region was only used to monitor the unscattered electrons.

The energy analysis of the electron spectrum is obtained using standard time-of-flight (TOF) techniques. The scattered and secondary electrons are allowed to drift for 432 mm in the field-free region between the scattering center and a graphite-coated copper grid (94% optical transmission) located 6 mm in front of the surface of the electron detector, which consisted of two microchannel plates (MCP) arranged in a chevron configuration. The electrons were accelerated by 253 V between a graphite-coated copper grid and the front surface of the MCP. The relative efficiency of this detector (grid and MCP combination) for electrons was measured to within 2%.[14] The angular acceptance of 1.5° of the detector was determined by an aperture of 2 mm diameter at a distance of 74 mm from the scattering center. The magnetic field around the apparatus was reduced to less than 1 mG by use of a Helmholtz coil pair and μ-metal shields. The electronics used in this experiment were the same as used in Ref. 1.

The procedure for data collection was identical to the one used for helium.[1] A time-of-flight spectrum S of electrons of all energies, scattered and ejected, was measured for a time period t_1 at a constant angle for a selected primary energy. The gas flow was then diverted into a tube, located 6 cm from the scattering center, to reproduce the background pressure ($\sim$42 μTorr). A background spectrum S_b was taken for a duration t_2. The background spectrum was then multiplied by t_1/t_2 and subtracted from S. We denote this difference by I_{sc}. This background subtraction was done for all angles and primary energies presented. The procedure for placing the spectra measured at different angles for a selected primary energy on a relative scale by use of short time scans is presented in Ref. 1 and was employed here. In these measurements the total photon yield from fluorescence was found to be isotropically distributed and was used as a check on the relative scale normalization. The photon yield was higher than in the case of helium.

The conversion from the background-subtracted TOF spectrum I_{sc} to the DDCS was carried out by use of the relation

$$\frac{d^2\sigma}{dW d\Omega}(W,\theta)=\frac{I_{sc}}{\eta(W)\epsilon(W)(dW/dt)}c\ , \tag{1}$$

where dW/dt is a function of the flight length L and flight time t given by $dW/dt=-(m/e)L^2/t^3$, $\eta(W)$ is the relative detector efficiency, $\epsilon(W)$ is the fractional attenuation of the scattered electron current of energy W by the rest gas, and c is a proportionality constant. The attenuation correction was modeled by use of Beer's law and for $W>4$ eV was typically less than 6%. At 2 eV it was $\sim$12%. The total cross sections for N_2 needed in the estimation of $\epsilon(W)$ were taken from Refs. 15 and 16. The total cross sections needed at 1 and 2 keV were estimated from the data in Ref. 16 by use of the Bethe-Born formula.[17]

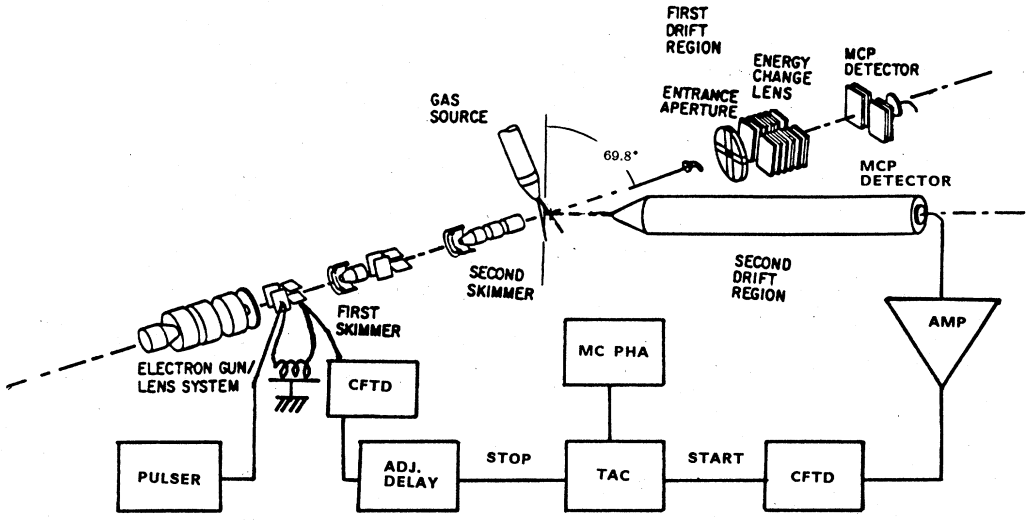

FIG. 1. Schematic view of the pulsed electron beam time-of-flight apparatus. The second drift tube moves in a horizontal plane about the scattering center and the electron beam direction is 69.8 deg with respect to the rotation axis. CFTD stands for constant fraction timing discriminator; STOP and START are the stop and start inputs to the time to amplitude converter, TAC; MCPHA is a multichannel pulse-height analyzer and AMP stands for amplifier.

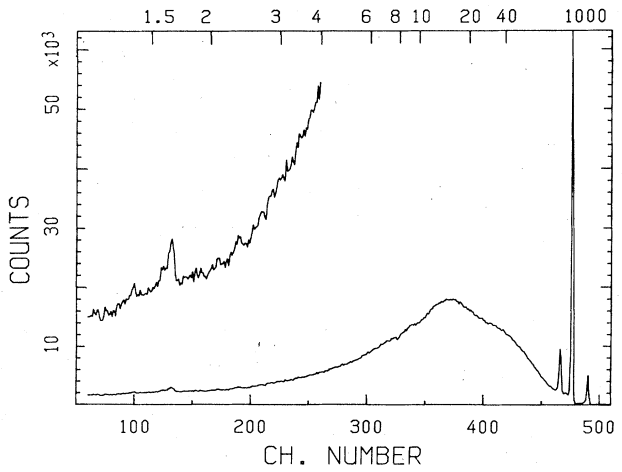

FIG. 2. A typical time-of-flight spectrum obtained using 1000-eV electrons incident on molecular nitrogen at a scattering angle of 150 deg. The lower horizontal scale is given in channel numbers which are linearly related to time of flight and the upper horizontal scale shows the scattering energy in eV. The low-energy portion of the spectrum is replotted after multiplication by a factor of 10 to show the 1.6 eV autoionization line.

In Fig. 2 a typical TOF spectrum obtained at 150° scattering angle and 1000-eV primary energy is shown. Notice the intense narrow peak centered at the primary energy due mainly to elastic electron scattering. This peak will be referred to as the elastic line and appears to have an energy width of about 250 eV (at 1000 eV) due to the time per channel width used. To the right of this peak there is another peak corresponding to a flight time of ~ 1.5 ns due to photons. To the left of the elastic line, a feature due to (KLL) Auger electrons[18] at around 362 eV and a broad peak with some discernible structure due to autoionization lines at ~ 7 and 9 eV can be seen. A prominent peak of 0.05 eV energy width at 1.6 eV is also due to autoionization. Details on the origin of these autoionizing features will be discussed in Sec. IV.

A primary energy was selected and the measurements were made at different angles of ejection. Because of the finite time per channel width used (1.6 ns) and the full width at half maximum (FWHM) of the electron pulse (1 ns) the "elastic line" contains both true elastic events and inelastic energy-loss events within the effective energy resolution of the experiment. The elastic line intensity was corrected at each θ for inelastic scattering by use of the procedure outlined in Ref. 1. By use of Eq. (1) the relative DDCS at each angle was determined after placing the spectra at different angles on the same relative scale. The relative corrected elastic DCS's were normalized to selected absolute measurements to place the measurements on an absolute scale. This was carried out at each primary energy.

The estimated uncertainties in the present DDCS's are essentially the same as those presented in Ref. 1. For convenience a summary of the estimated errors is presented in Table I for N_2. The present DDCS error estimates do not include allowance for possible transmission loss at low ejected energy. The transmission loss varies smoothly from onset at less than 4 eV to complete cutoff at less than 0.4 eV. Our results in this range are expected to be lower bounds to the true values.

TABLE I. Percentage error estimates for the DDCS.

Electron energy (eV)	$\delta(dt/dW)$	$\delta(\epsilon(W))$	Magnetic field effect	Overall[a,b] percentage error
2	1.6	4.6	2.8	$-10, +13$
4	1.7	2.4	2.0	$-10, +12$
6	1.8	2.0	1.6	$-10, +12$
8	1.8	2.0	1.4	$-10, +12$
10	1.8	2.1	1.3	$-10, +11$
16	2.0	2.3	1.0	$-10, +11$
20	2.1	2.4	0.9	$-10, +11$
40	2.5	2.1	0.6	$-10, +10$
50	2.8	2.0	0.6	$-10, +10$

[a]The other energy-independent errors are $\delta(\Delta t)=0.5\%$ and $\delta(\eta(W))=2\%$. Relative scale error is 6%, the normalization error is 6%, and the count rate error is 3%.
[b]All the errors are added quadratically except the magnetic field effect which decreases the DDCS. This error was included asymmetrically.

III. RESULTS AND DISCUSSION

The results of the DDCS for different primary energies are presented in four parts. Comparisons with the present normalized elastic DCS and total ionization cross section at each primary energy with other measurements are presented.

A. 200-eV primary electrons

The experiments were carried out at ejection angles from 30° to 150° in steps of 15°. The experiment was repeated at ejection angles of 45°, 60°, and 135°. The present

TABLE II. The estimated values for the percentage of inelastic scattering contributing to the "elastic" line intensity at different angles, θ, and primary energies, T.

θ (deg)	Percentage of inelastic scattering T (eV) 200	500	1000	2000
30	2	18	18	14
45	2	15	9	12
60	2	14	7	6
75	2	15	6	7
90	2	15	7	8
105	2	17	6	9
120	2	19	8	11
135	2	15	5	13
150	2	16	6	12

TABLE III. Comparison of the present elastic DCS for 200 eV electrons with other results. All values are in units of 10^{-19} cm^2/sr. The scattering angle is denoted by θ. The values enclosed in square brackets are interpolated results.

θ (deg)	Present results	Shyn & Carignan[a]	DuBois & Rudd[b]	Jansen *et al.*[c]	Herrmann *et al.*[d]
30	440.0	456.0	409.0	440.0	410.0
45	160.0			176.0	170.0
60	96.0	96.0	100.0		98.0
75	60.0				56.0
90	46.5	[43.0]	46.0		43.5
105	53.0				[45.4]
120	55.0	48.0	51.0		49.1
135	54.0				48.5
150	57.0	[51.0]	50.0		

[a]Reference 20.
[b]Reference 21.
[c]Reference 19.
[d]Note that the normalization adopted by the authors of Ref. 22 (Table II) has been used.

relative elastic DCS was normalized by the procedure discussed in Ref. 1. The method involves finding an average scale factor by matching the relative DCS to the selected absolute elastic DCS, usually at two or three angles, to minimize the scaling error. For normalization of the 200-eV results we selected the absolute measurements by Jansen *et al.*[19] at 30 and 45 deg. At 200-eV primary energy, the energy resolution in the present experiment is 20 eV. This insures a small correction for the inelastic contribution. Our estimation procedure[1] for the inelastic contribution to the "elastic" line was employed for all angles and the correction was found to be 2% independent of angle. These estimated percentage corrections for this and other primary energies are summarized in Table II. The present normalized elastic DCS was compared to the measurements by Shyn and Carignan,[20] DuBois and Rudd[21] and with the scaled relative measurements by Herrmann *et al.*[22] in Table III.

Table III shows fair agreement between the present results and those by DuBois and Rudd[21] in both shape and magnitude. A shallow minimum in the elastic DCS occurring around 90 degrees in the data by Dubois and Rudd[21] is also observed in the present experiment. The relative measurements by Herrmann *et al.*[22] are normalized to the 50 deg measurement of Jansen *et al.*[19] There is again fair agreement between these results and those of the present experiment.

The absolute DDCS at 2, 4, 6, 8, 10, 20, and 40 eV ejected energies are given in Fig. 3 along with the measurements by Shyn[11] and OBP.[3] The present measurements are denoted by circles, the results of Shyn are shown by squares and the OBP results by $\times$'s. The solid line is a least-square fit to the expansion

$$\frac{d^2\sigma}{dW d\Omega} = \sum_{n=0}^{4} A_n P_n(\cos\theta) , \tag{2}$$

where P_n is the nth-order Legendre polynomial, θ is the scattering or ejection angle, and the A_n's are constants to be determined by least squares and are functions of the primary T and ejected W energies.

Notice the large increase in the DDCS in the forward direction starting from about 45 deg ejection angle in Shyn's data. The present results do not show this behavior. It is of interest to note that at θ greater than 80 deg, the data of Shyn tend to look similar to the present results. The agreement in shape of the angular distributions between these two experiments gets better with increasing ejected energy. At $W=40$ eV the agreement in shape extends to lower ejection angle. As the forward peak in Shyn's data becomes less prominent at higher ejected energies, their data tend to agree better at lower scattering angles with the present results.

The forward peak in Shyn's data for N_2 is more prominent than for He and extends to higher ejection angles. In this case our data conclusively rules out the existence of forward peaking in our angular range of observation. In the case of helium[1] our results were merely suggestive of the absence of a forward peaking.

The angular distributions of the DDCS by OBP are more strongly angle dependent than the present results. At small and large angles of ejection OBP data are lower than the present results. At ejected energies of 6, 8, and 10 eV OBP results show an enhanced binary-peak-like structure centered at lower ejection angles than the same peak in the present results. By 20 eV the shift has largely disappeared. At 40 eV the OBP results are in good agreement with the present results except at the extreme angles. Note that the OBP data may be flawed at small and large angles due to lack of consideration of the proper electron and gas beam geometries as pointed out by DuBois and Rudd.[4]

The DDCS were integrated over the ejection angles to obtain the single-differential cross section (SDCS), $d\sigma/dW$. This integration when carried out using the fitted form of the DDCS given by Eq. (2) gives

$$\frac{d\sigma}{dW} = 4\pi A_0 , \tag{3}$$

with A_0 being the zeroth-order coefficient in Eq. (2). The SDCS is converted into a Y function by dividing it by the Rutherford cross section. Unlike the case of helium, molecular nitrogen has five different ionization energies leading to the formation of N_2^+. These are[23] 15.6, 16.9, 18.7, 37.3, and 409.5 eV. For 200-eV primary electrons the last ionization channel is closed. Hence for nitrogen there are a variety of ways to define the necessary Rutherford cross section. A discussion of these possibilities has been given by Kim.[10] Here we take the lowest ionization energy in defining the Rutherford cross section. The formula for Y which is a function of the energy loss, E

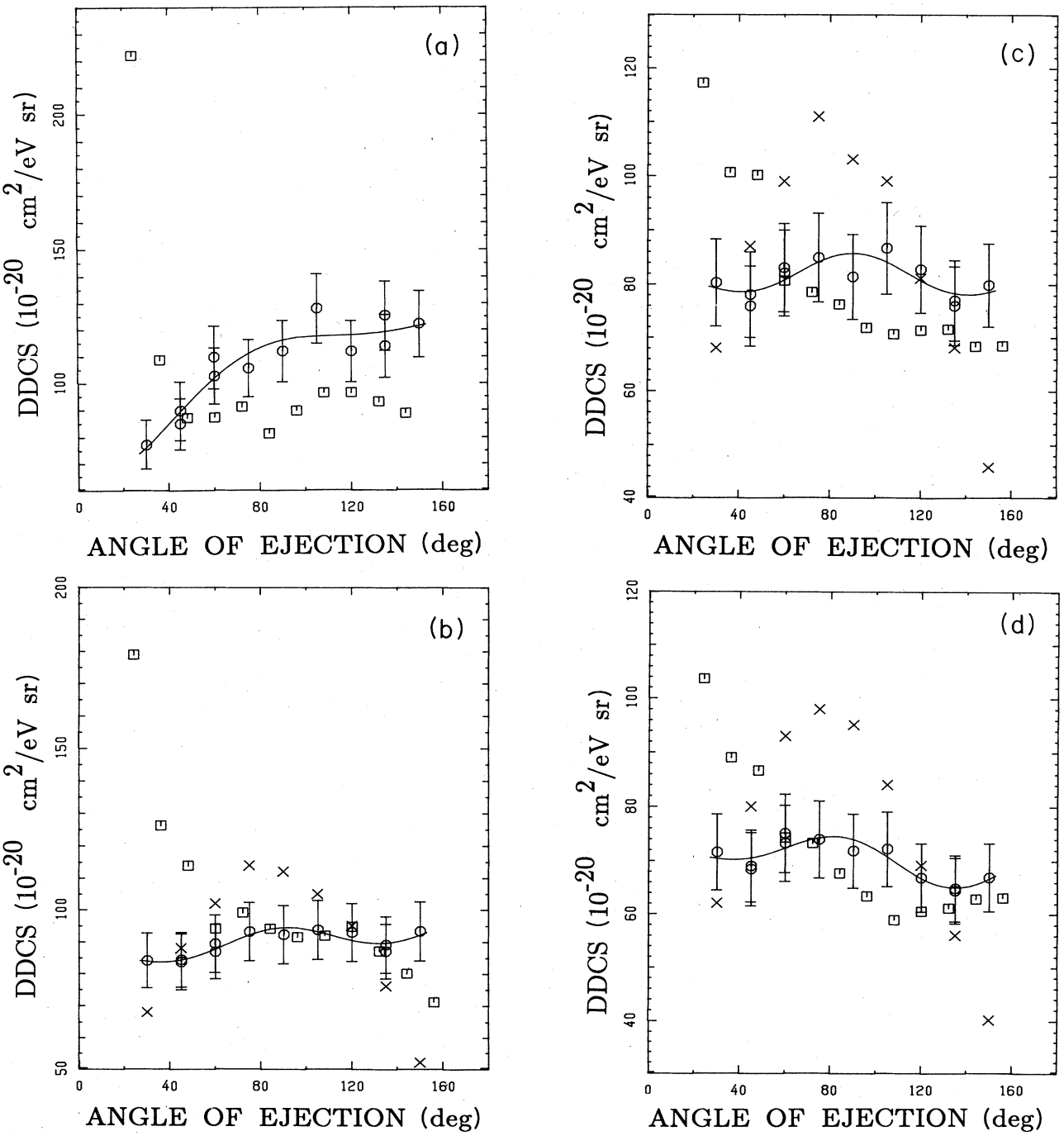

FIG. 3. Absolute DDCS for N_2 at a primary energy of 200 eV. The circles denote the present measurement. The squares represent the results of Shyn; the $\times$'s represent the results of OBP; the solid line is a fit to an expansion in Legendre polynomials using the present data. The measurements at 2, 4, 6, 8, 10, 20, and 40 eV ejected energy are designated by $a, b, \ldots, g$, respectively.

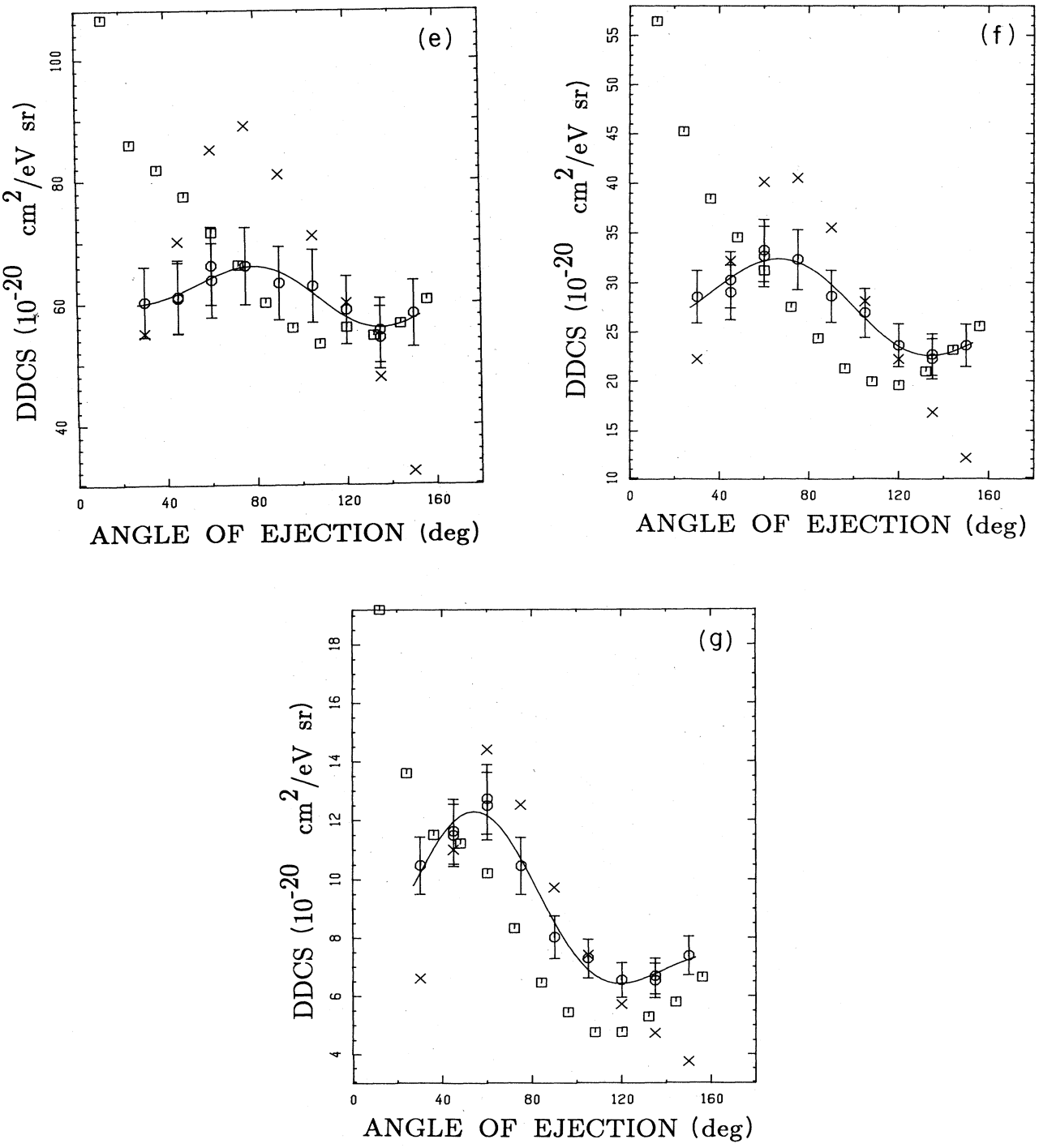

(*Continued*). FIG. 3.

$(= W + 15.6$ eV), and primary energy T is given as

$$Y(E,T)=(d\sigma/dW)/(d\sigma_R/dE)\ ,$$

where

$$\frac{d\sigma_R}{dE}=\frac{4\pi a_0{}^2}{T}\frac{E^2}{R^2}\ . \tag{4}$$

In Eq. (4) a_0 is the Bohr radius and R is the Rydberg unit of energy. A plot of Y versus R/E, called the Platzman plot, for all the primary energies is given in Fig. 4.

At 200-eV primary energy the extrapolated value for Y, ignoring the fast rising tail, for large ejected energies is approaching a value of about 10. This limiting value represents the effective number of target electrons in-

volved in the ionization process. The obvious features due to autoionization and shape resonances in the Platzman plot are discussed in Sec. IV.

The Y curve is bounded by the two limits, X_1 $[=2R/(T+15.6)]$ and X_2 $(=R/15.6)$ corresponding to the ejected electron energies of $(T-15.6)/2$ and 0 eV. These limits are indicated by vertical boundaries in Fig. 4.

For 200-eV primary energy, the Y values just below X_1, rise very rapidly as evident from Fig. 4. This rise is due primarily to exchange effects between the scattered and ejected electrons. To compute the total ionization cross section, σ_{ion}, the Y curve was extrapolated, where necessary, on either side of the broad peak by fitting the experimental points to a curve of the type

$$Y=\frac{a}{b+(R/E)^{\alpha}}\ , \tag{5}$$

with $\alpha=2$ (-2) for left (right) portions of the experimental curve. The fitted curves are also shown in Fig. 4. The extrapolated values read off from the fitted curve were used from X_1 to 0.115 and from 0.773 to X_2 along with the experimental values in the intermediate region to integrate Y between the kinematic limits X_1 and X_2. The total ionization cross section σ_{ion} is calculated using the formula

$$\sigma_{\text{ion}}(T)=4\pi a_0^2\left[\frac{R}{T}\right]\int_{X_1}^{X_2} Y(E,T)d(R/E)\ . \tag{6}$$

The constants in Eq. (5) for the low-energy side of the Y plot were determined by least squares in the R/E range 0.550—0.653. The error due to other choices of determining the parameters, such as use of the region above 0.653 would lead to a 3% uncertainty in σ_{ion}. For 200-eV primary energy only the extrapolated values on the low-energy side were used as the experimental points cover the rest of the region. At other primary energies the extrapolated values on both high- and low-ejected-energy regions were employed.

The σ_{ion} derived from the present experiment is shown in Table IV along with the values for other primary energies. At 200 eV electron energy there is excellent agreement between the present measurement and that by Rapp and Englander-Golden.[24] The results of OBP (Ref. 3, p. 214, Table I) and Shyn (Ref. 11, Fig. 6) are also in agreement with the present result.

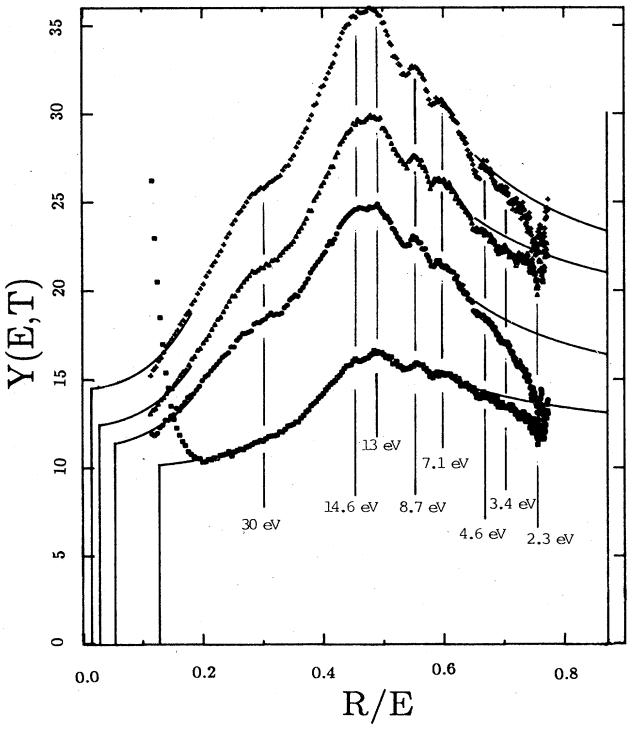

FIG. 4. Platzman plot of the single differential cross section expressed as $Y(E,T)$ vs R/E where R is the Rydberg unit of energy, E is the energy loss ($W+15.6$ eV), and T is the primary energy. See Eq. (4) and the associated text for a definition of Y. The right and left boundaries of Y correspond to ejected electron energies of zero and $(T-15.6)/2$ eV, respectively. Note the features due to autoionization and shape resonances. The energies corresponding to the vertical lines which mark features explained in the text are shown. The measurements at 200, 500, 1000, and 2000 eV incident energy are plotted from bottom to top in the graph.

B. 500-eV primary electrons

At this impact energy the experiment was carried out at scattering angles in the range of 30° to 150° in steps of 15°. The experiment was repeated at 90°. The relative elastic DCS determined from the TOF spectra were normalized against the values reported by Bromberg at 45°, 60°, and 90°. The present normalized elastic DCS is compared to the measurements by Bromberg,[25] Kambara and Kuchitsu,[26] Dubois and Rudd,[21] Herrmann *et al.*,[22] and Jansen *et al.*[19] in Table V. In the overlapping region the present measurements are in excellent agreement with those by Bromberg.[25] The results of Kambara and Kuchitsu[26] are larger at backward angles than the present measurements. The measurements by DuBois and Rudd[21] are in good agreement with the present values. The values by Herrmann *et al.*,[22] if normalized to Bromberg's results at 90 deg, agree with the present measurements.

The present DDCS's for $W=2$, 4, 10, 20, and 40 eV are presented in Fig. 5. The circles, triangles, and crosses ($\times$'s) denote the present experiment, results of DuBois and Rudd,[4] and those by OBP (Ref. 3), respectively. The solid line is a fit to an expansion of the DDCS in Legendre polynomials. At 2 eV ejected energy there are no experimental values for comparison. The 2-eV data appear to suffer from transmission problems as can be guessed from the Y plot in Fig. 4. At 4 eV the differences between the present measurement and those by OBP are the same as they were for 4 eV at 200-eV primary energy. This trend continues up to about 10 eV. At $W=20$ eV the OBP results are in agreement with the present results except at the extreme angles of 30 and 150 deg. Further, in the backward angles of ejection the OBP results tend to

TABLE IV. Comparison of the total ionization cross section, σ_{ion}, obtained in the present experiment with literature values. The primary energy, T, is given in eV and σ_{ion} is in units of 10^{-16} cm^2.

Measurement	σ_{ion} (10^{-16} cm^2) Primary energy (eV) 200	500	1000	2000
This experiment	2.42±0.24	1.42±0.14	0.88±0.09	0.52±0.05
Rapp and Englander-Golden[a]	2.27±0.16	1.45±0.10	0.92±0.06	
OBP[b]	2.43±0.61	1.42±0.36	0.83±0.21	0.46±0.12
DuBois and Rudd[c]		1.21±0.18		
Shyn[d]	2.5±0.45			

[a]Reference 24.
[b]Reference 3.
[c]Reference 4.
[d]Reference 11.

TABLE V. Comparison of the present elastic DCS for 500 eV electrons with other results. All values are in units of 10^{-19} cm^2/sr. The scattering angle is denoted by θ. The values enclosed in square brackets are interpolated results.

θ (deg)	Present results	Bromberg[a]	Kambara & Kuchitsu[b]	Dubois & Rudd[c]	Jansen *et al.*[d]	Herrmann *et al.*[e]
30	292.0	285.0	285.0	278.0	286.0	281.0
45	84.0	85.0	82.0		87.0	82.1
60	41.3	40.9	41.2	40.0		38.8
75	23.2	[23.7]	[24.5]	[23.7]		22.0
90	14.5	14.8	16.0	14.7		13.5
105	11.2	[11.8]	[13.4]	[12.2]		[10.7]
120	8.4		11.1	9.4		8.4
135	7.9		[10.5]	[8.3]		7.2
150	7.6		10.0	8.2		

[a]Reference 25.
[b]Reference 26. The relative measurements are normalized at 30° to the results given in Ref. 25.
[c]Reference 21.
[d]Reference 19.
[e]Note that the normalization adopted by the authors of Ref. 22 (Table II) has been used.

TABLE VI. Comparison of the present experimental elastic DCS for 1000 eV electrons with literature values. The scattering angle is denoted by θ. All values are in units of 10^{-19} cm^2/sr.

θ (deg)	Present experiment	Theory[a]	Jansen *et al.*[b]	Herrmann *et al.*[c]
30	119.0	141.0	133.0±8.0	121.0
45	36.3	40.5	37.8±2.3	35.1
60	13.5	15.1		12.5
75	7.8	[8.4]		6.7
90	4.80	5.2		4.06
105	3.40	[3.61]		[2.81]
120	2.58	2.72		2.18
135	2.19	2.34		1.87
150	1.96	1.99		

[a]Calculation based on the independent atom model using partial-wave amplitudes given in Ref. 28.
[b]Reference 19.
[c]Note that the normalization adopted by the authors of Ref. 22 (Table II) has been used.

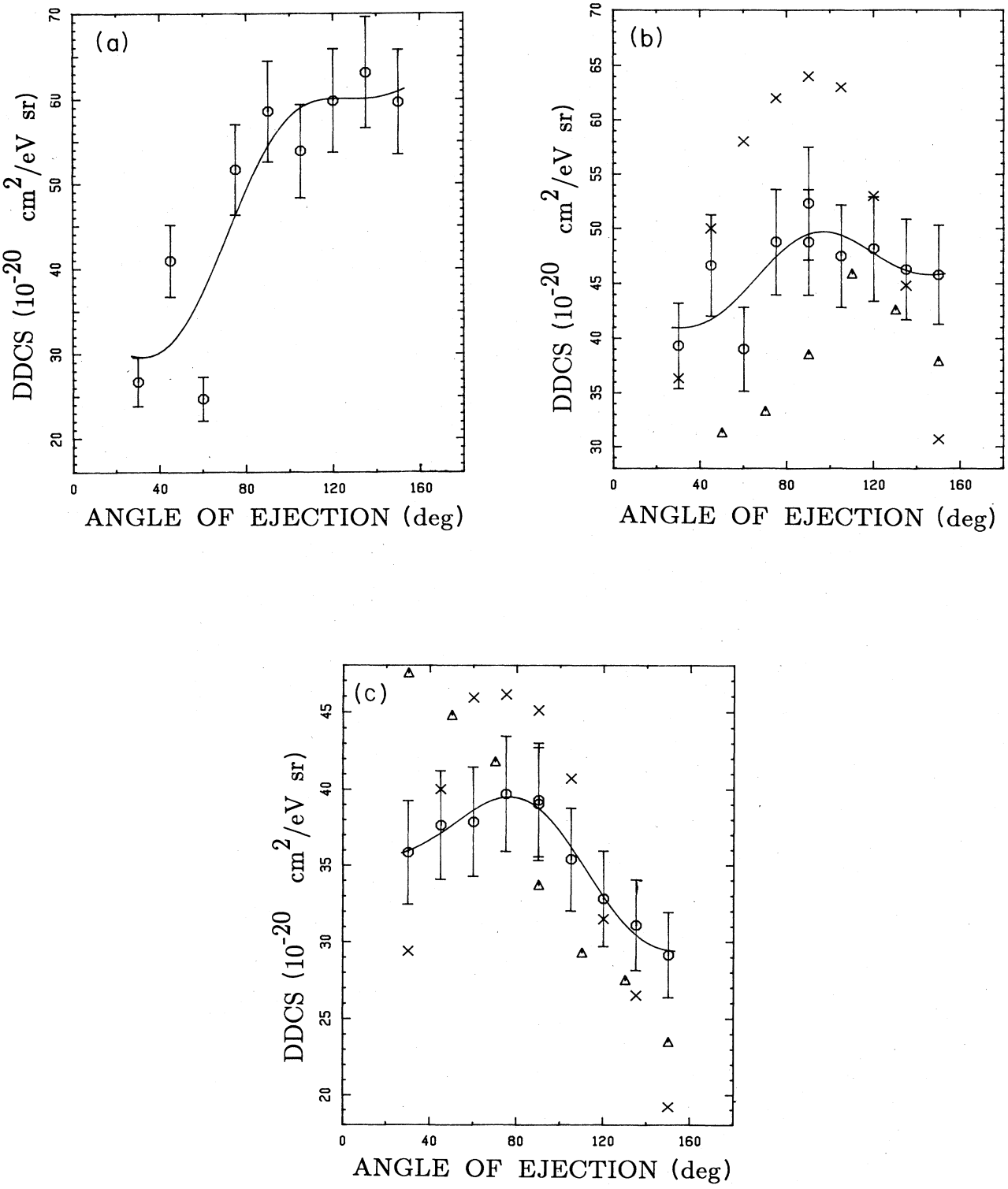

FIG. 5. Absolute DDCS for N_2 at a primary energy of 500 eV. The circles denote the present measurement. The triangles represent the results of DuBois and Rudd; the $\times$'s represent the results of OBP; the solid line is a fit to an expansion in Legendre polynomials using the present data. The measurements at 2, 4, 10, 20, and 40 eV ejected energy are designated by $a, b, \ldots, e$, respectively.

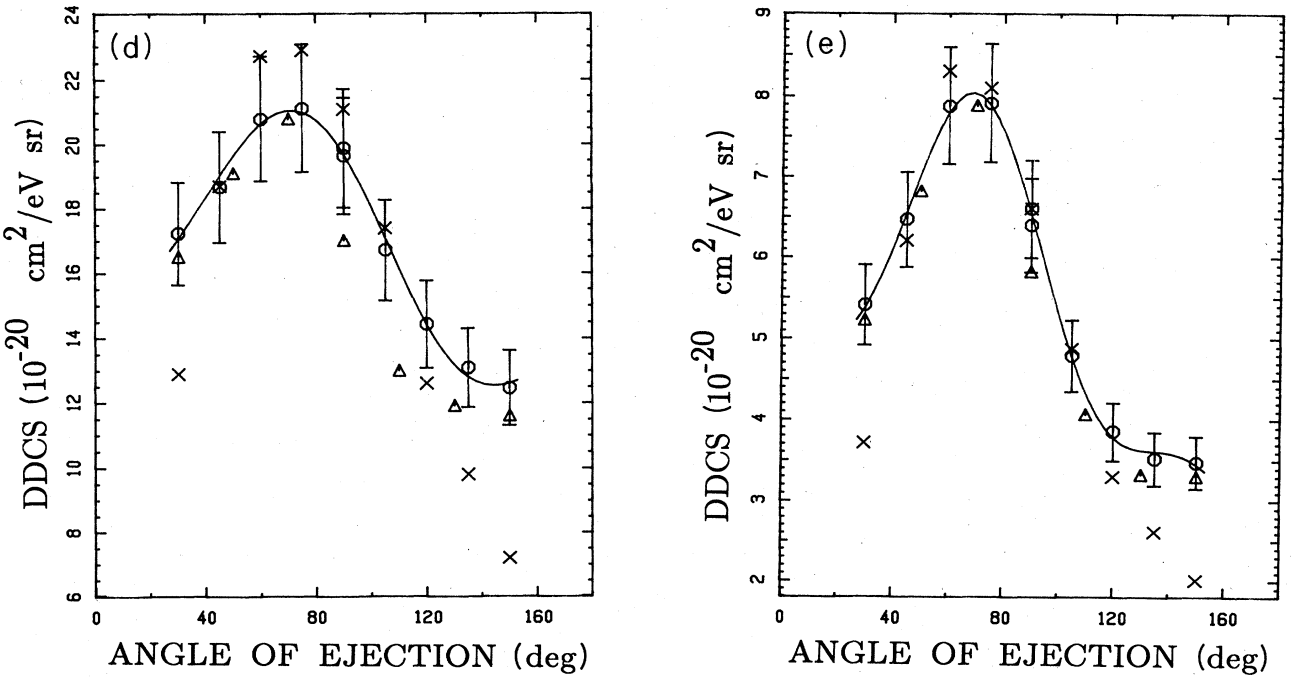

FIG. 5. (*Continued*).

fall much faster than the present results. At 40 eV the agreement between these two experiments shows further improvement except at the extreme angles. At 10 eV the DuBois and Rudd results are in agreement in shape in the backward angles, however, at angles below $\sim 80°$ they do not decrease as the present results do but continue to increase suggesting the existence of a forward peak. At 4 eV their results do not show any regularity in the angular distribution. At 20 and 40 eV of ejected energy the DuBois and Rudd results are in excellent agreement with ours. The estimated accuracy in their measurement was $\pm 15\%$ and they indicated that their low-ejected-energy cross sections might be unreliable.

The total ionization cross section deduced from the present measurement is given in Table IV along with comparisons with other values. Again, the present result is in agreement with other values.

C. 1000-eV primary electrons

The experiment was carried out at this primary energy in the angular range of 30° to 150° in steps of 15°. The experiment was repeated at scattering angles of 60°, 90°, and 150°. The relative elastic DCS was normalized to the absolute measurements by Jansen *et al.* at 30° and 45°. The normalized elastic DCS is presented in Table VI and the values are compared to those given in the literature. The relative measurements of Herrmann *et al.*[22] were normalized as indicated in Ref. 22. These measurements are 10% lower than the present measurements for $\theta > 60°$. The elastic DCS was computed in the independent-atom model[27] (IAM) using the partial-wave amplitudes of Fink and Ingram[28] and values are also given in the table for comparison. The agreement between this theory and the present experiment is good.

The DDCS at this primary energy was measured by OBP (Ref. 3) and by Oda *et al.*[7] The latter authors did not give any numerical values and there appear to be some[29] typographical errors in the text. Figure 2 in their paper gives a perspective diagram of the DDCS as a function of angle and energy. Because of the difficulty in obtaining reliable values from such a graph no comparisons of the present data with that by Oda *et al.* were attempted. In Fig. 6 the present DDCS measurements at ejected energies of 2, 4, 10, 20, and 40 eV are presented. The circles in these figures are the present measurements while the $\times$'s are the data by OBP. The solid line is a least-square fit to an expansion in Legendre polynomials of the DDCS. At $W=4$ eV the OBP results for ejection angles greater than 50° are in fair agreement with the present results. However, the OBP results below about 50 deg drop below ours. The present results are generally higher by about 10% than the OBP results. At $W=10$ eV the OBP results are lower than the present measurements at 30° and 150°. The discrepancy is greater at 30° than at 150°. At other angles, the agreement is quite good. With increasing ejected energy the disagreement at 30° and 150° continues with the DDCS at 150° lying lower than the 30° measurement. This suggests that the DDCS at a constant angle as a function of ejected energy for the present experiment is different from that by OBP. Again at $W=20$ and 40 eV the agreement between the present experiment and OBP's is quite good except at the extreme angles of ejection.

The total ionization cross section σ_{ion} at this primary

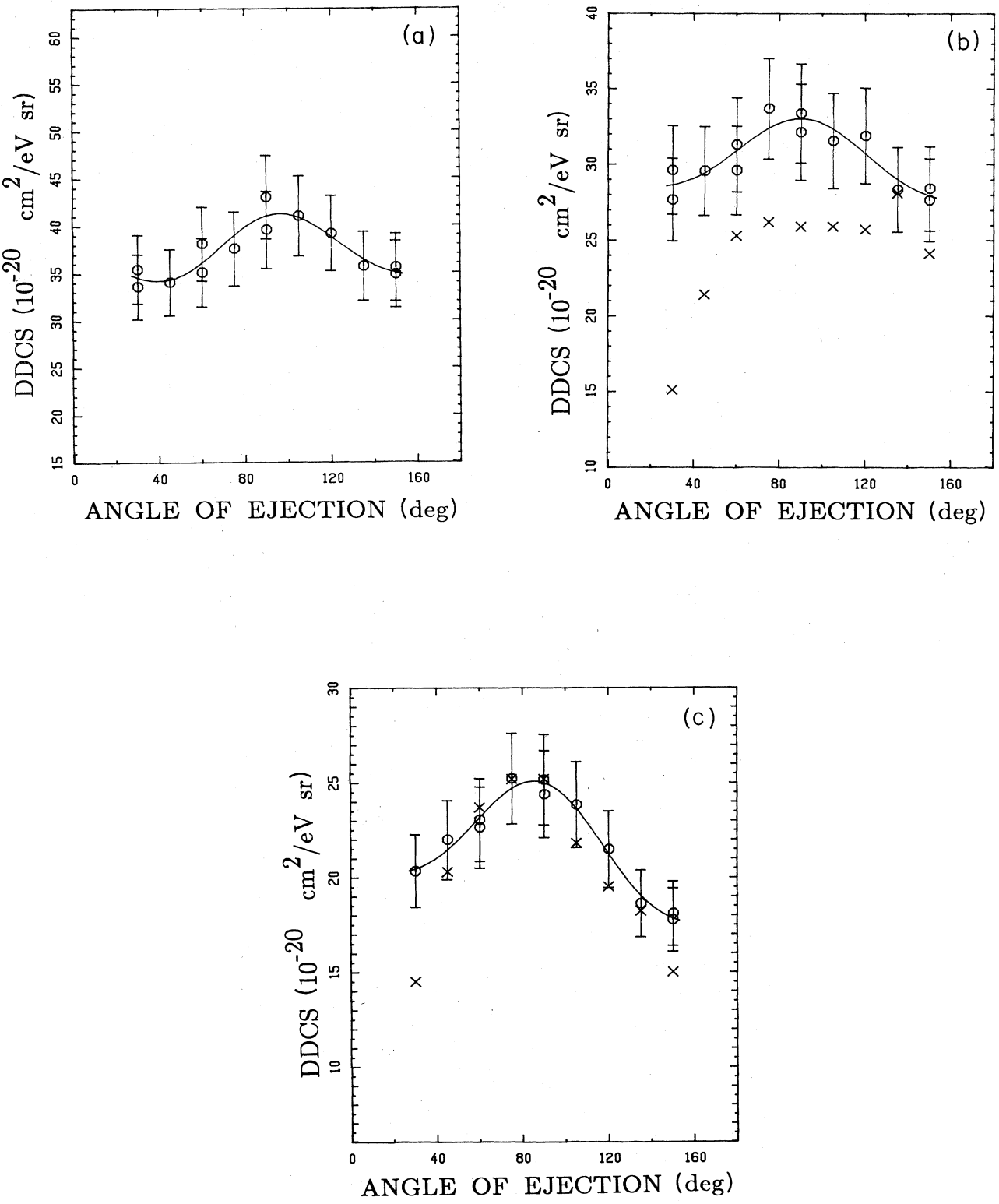

FIG. 6. Absolute DDCS for N_2 at a primary energy of 1000 eV. The circles denote the present measurement. The $\times$'s represent the results of OBP, the solid line is a fit to an expansion in Legendre polynomials using the present data. The measurements at 2, 4, 10, 20, and 40 eV ejected energy are designated by $a, b, \ldots, e$, respectively.

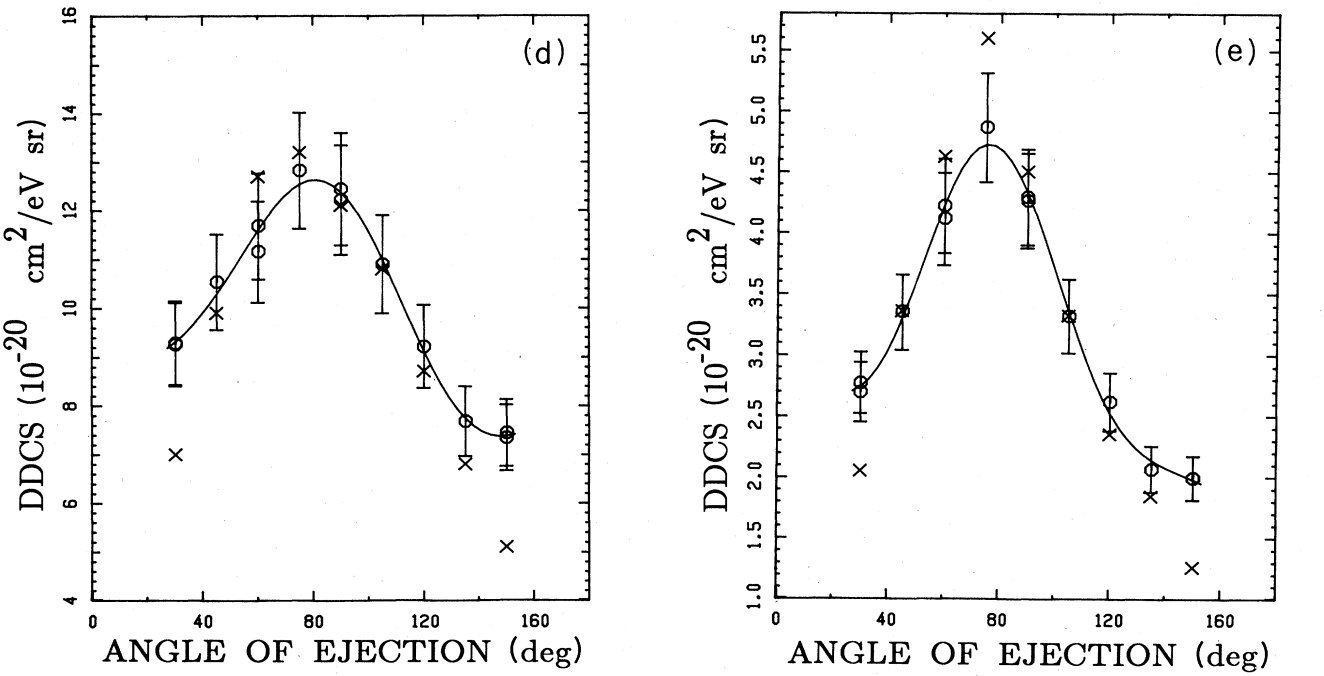

FIG. 6. (*Continued*).

energy is calculated and is given in Table IV. The present result is in good agreement with that of Rapp and Englander-Golden[24] and OBP.

D. 2000-eV primary electrons

At this primary energy the experiment was carried out in the angular range of 30° to 150° in steps of 15°. The experiment was repeated once at 90° and twice at 135°. The whole experiment was repeated once more a year later. The newer experiment was done only at 30°, 45°, 60°, 90°, 120°, and 150° of scattering angle with one repeated measurement at 30° and 90° and two at 60°. The reproducibility of the experiment was excellent (±6%) except at the lower ejected electron energies ($W<4$ eV). Altogether there were 22 independent data sets obtained at this primary energy.

The relative elastic DCS was normalized to the data of Jansen *et al.*[19] at 30° and 45°. The present normalized elastic DCS and IAM elastic DCS are presented in Table VII along with the measurements by Jansen *et al.* The IAM values are in excellent agreement with the absolute measurements of Jansen *et al.* at 30° and 45° and are in quite good agreement with the present values at all angles.

The DDCS at 2, 4, 10, 20, and 40 eV of ejected energy are shown in Fig. 7 with the present results denoted by circles. Comparisons are made with the values reported by OBP (indicated by ×'s). The solid line in these figures is the result from a least-squares fit to a Legendre polynomial expansion of the DDCS. Transmission losses of as much as 50% were detected in the earlier experiments at 2 eV ejected energy. The low-transmission results are not shown in Fig. 7(a). At 4 eV the excellent reproducibility of all the measurements taken over a period of one year can be noted. The OBP data are lower than the present values at most angles, especially at 30° and 45°. The difference in the angular shapes between these two measurements at this primary energy is quite similar to that at 1000 eV. At 10 eV ejected energy there is good agreement between the present results and those by OBP at all angles of ejection except at 30° and 150°. This agreement is present for $W=20$ and 40 eV as well. As in the case of 1000-eV primary energy, the DDCS at 30 deg of OBP seems to agree better for higher ejected energy while the 150 deg data continue to be low.

TABLE VII. Comparison of the present experimental elastic DCS for 2000 eV electrons with literature values. The scattering angle is denoted by θ. All values are in units of 10^{-19} cm^2/sr.

θ (deg)	Present experiment	Theory[a]	Jansen *et al.*[b]
30	45.0	46.8	45.1±3.2
45	11.3	11.80	12.0±8.4
60	4.37	4.58	
75	2.16	2.25	
90	1.35	1.33	
105	0.88	0.92	
120	0.63	0.66	
135	0.51	0.53	
150	0.406	0.442	

[a]Calculation based on the independent atom model using partial-wave amplitudes supplied by Fink. (Unpublished results for atomic nitrogen. Values at other incident energies can be found in Ref. 28.)
[b]Reference 19.

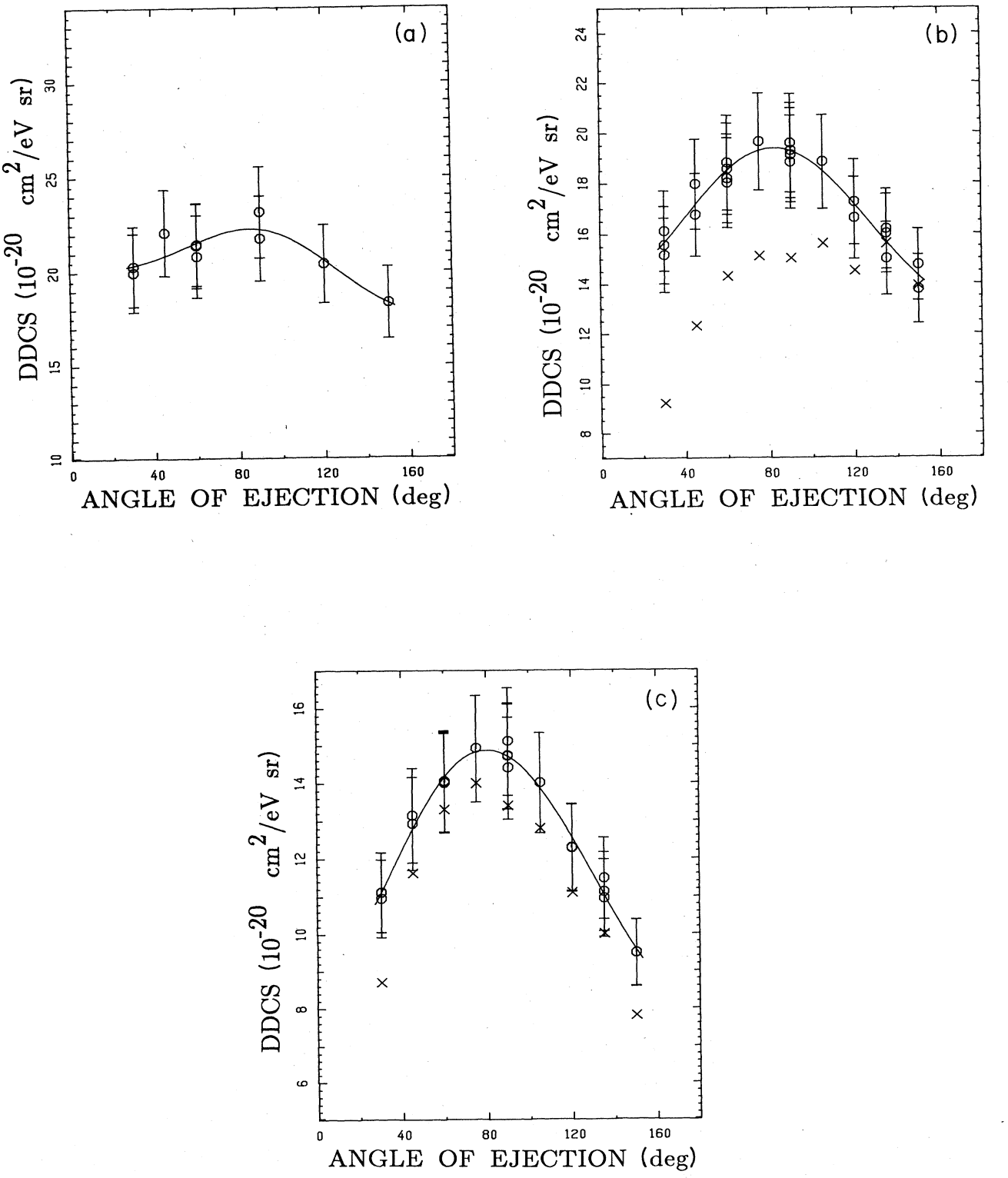

FIG. 7. Absolute DDCS for N_2 at a primary energy of 2000 eV. The circles denote the present measurement. The $\times$'s represent the results of OBP, the solid line is a fit to an expansion in Legendre polynomials using the present data. The measurements at 2, 4, 10, 20, and 40 eV ejected energy are designated by $a, b, \ldots, e$, respectively.

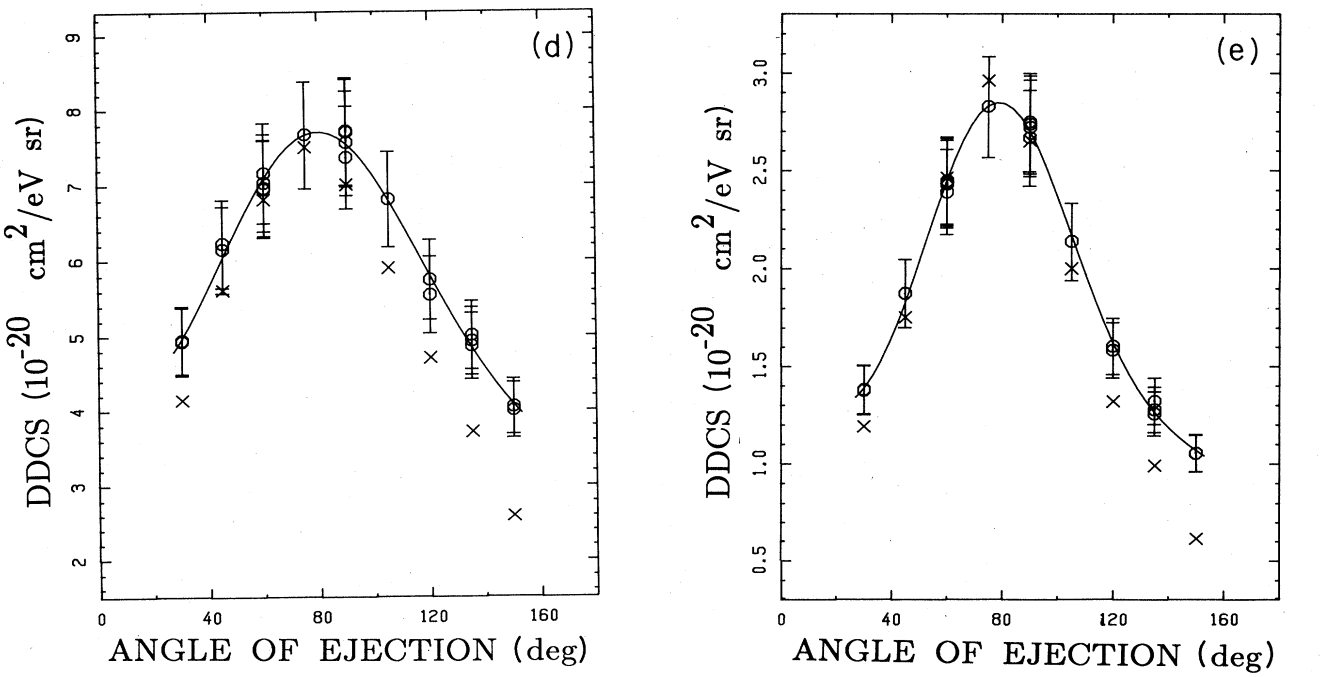

FIG. 7. (*Continued*).

The total ionization cross section is calculated and is given in Table IV. There is excellent agreement between the present measurement and the value deduced from the data of Ref. 3.

IV. AN ANALYSIS OF SPECTROSCOPIC FEATURES

A. The region above 2 eV

In the Platzman plot (Fig. 4), for all the primary energies a number of features are clearly discernable. To facilitate the assignment of these features we have plotted the available partial channel photoionization cross sections after the suggestions of Kim[10] as

$$F(W)=\sum_j \frac{E^2}{E_j}\frac{df_j(E_j)}{dE_j}=\sum_j F_j(W)\ , \tag{7}$$

where the summation is over the different orbitals of the target molecule, $E=W+15.6$ eV and $E_j=W+I_j$ with I_j the ionization potential of the jth channel. As the partial oscillator strength for ionization df_j/dE_j is given as a function of energy transfer (photon energy) the thresholds for all partial channel cross sections are translated to have a common origin at $W=0$ before the summation. In Figs. 8 and 9 we display the respective results for the synchrotron light source measurements of Woodruff and Marr[30] and Plummer *et al.*[31] The $X\,^2\Sigma_g^+$, $A\,^2\Pi_u$, and $B\,^2\Sigma_u^+$ ion channels are shown separately as well as summed using Eq. (7). Their overall scale is adjusted for comparison with our 2000-eV data (top curve in each case). Two other sets of data for separate channel photoionization cross sections exist. These are the results of Samson *et al.*[32] and Hammnet *et al.*,[33] not shown, which display general overall agreement in shape but the paucity of experimental points in the former study and lack of energy resolution in the latter did not permit determination of the detail obtained in our study. All show the broad feature at 12.7 eV and the peak at 7.1 eV. It should be

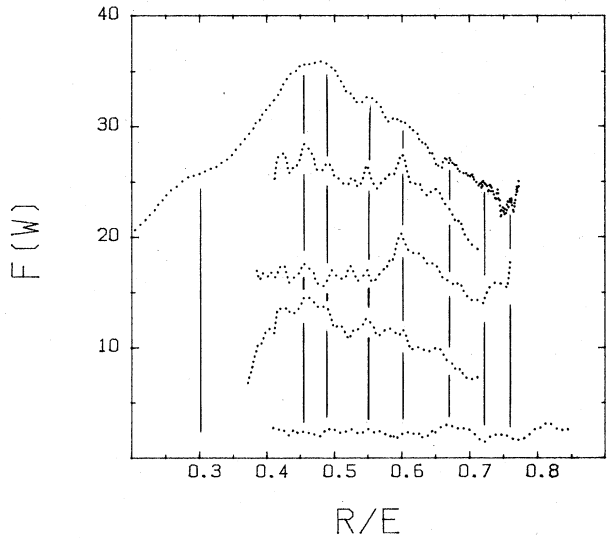

FIG. 8. The curves are from top to bottom: the $Y(E,2000)$ function from this work, $F(W)$ constructed from the photoionization data of Woodruff and Marr using Eq. (7) and scaled by the factor 0.9, $F_j(W)$ for the A photoionization channel scaled by the factor 1.2, $F_j(W)$ for the X photoionization channel, and $F_j(W)$ for the B photoionization channel. All $F_j(W)$ curves are derived from the data of Woodruff and Marr and are on the same relative scale (the scaling factors 0.9 and 1.2 were used only to separate the curves when plotted).

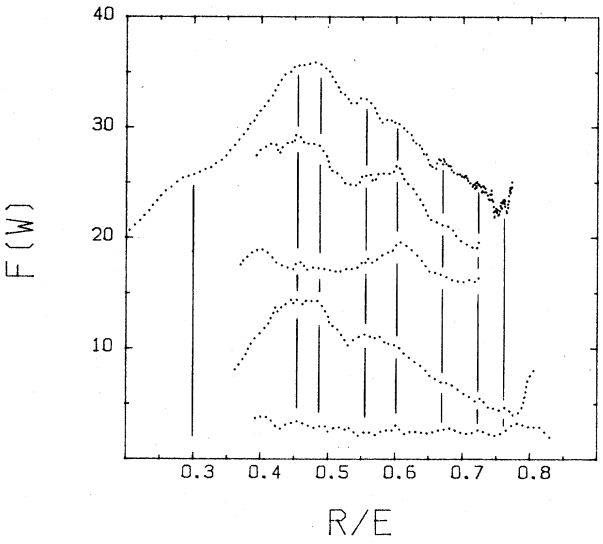

FIG. 9. The curves are from top to bottom: the $Y(E,2000)$ function from this work, $F(W)$ constructed from the photoionization data of Plummer *et al.* using Eq. (7) and scaled by the factor 1.2, $F_j(W)$ for the A photoionization channel scaled by the factor 1.2, $F_j(W)$ for the X photoionization channel, and $F_j(W)$ for the B photoionization channel. All $F_j(W)$ curves are derived from the data of Plummer *et al.* and are on the same relative scale (the scaling factor of 1.2 was used only to separate the curves when plotted).

kept in mind that only the studies of Woodruff and Marr[30] and Samson *et al.*[31] were carried out at the magic electron ejection angle of $\sim 54°$ while the other studies were carried out at 90°. In comparing the synchrotron studies with our work we have assumed that all features observed in these studies are real and not experimental artifacts or noise. In our own work it should be emphasized that the Y plot is the result of summing over 15 different angle-resolved spectra. Any random noise would be washed out in such a process hence we believe that all the structural features lying above the noise envelope of the data are real.

We note first that there seems to be a good correspondence between the features in the work of Plummer *et al.*[31] and Woodruff and Marr[30] if allowance is made for the difference in ejection angles used in the two studies. A second observation is that there seems to be a strong correlation between features observed in one channel and those in another. This would appear to be an example of channel coupling effects in the exit channels as observed previously in the case of SF_6 by Dehmer *et al.*[34] We also note that some features are slightly shifted in energy between the electron and synchrotron data. Assuming that both energy scales are correct, this could be due to contributions from nondipole allowed processes altering the slope of the Y function in our case.

The assignments of the main features are as follows. The structure in the peak at 14.6 eV comes about equally from the $X\,^2\Sigma_g^+$ and $A\,^2\Pi_u$ channels with the 12.7-eV peak coming mainly from the $X\,^2\Sigma_g^+$ channel. The feature at 8.7 eV comes from the $X\,^2\Sigma_g^+$ channel with evidence for some $A\,^2\Pi_u$ channel participation. The 7.1-eV peak is due to a feature in the $A\,^2\Pi_u$ channel with some contribution from the $X\,^2\Sigma_g^+$ channel. The feature at ~ 5 eV seems to be coming from the $B\,^2\Sigma_u^+$ channel. The feature at 3.4 eV does not appear in the Woodruff and Marr[30] data but can be seen only in the $X\,^2\Sigma_g^+$ channel of the data of Plummer *et al.*[31] The feature at 2.3 eV seems to come from the $X\,^2\Sigma_g^+$ channel with small contribution from the $B\,^2\Sigma_u^+$ channel as seen from the Plummer *et al.*[31] data. The Woodruff and Marr[30] data shows a smaller peak in the $B\,^2\Sigma_u^+$ channel and a larger peak in the $A\,^2\Pi_u$ channel but they occur midway between the 2.3 and 3.4 eV features in our data.

So far we have not discussed the shoulder occurring at ~ 30 eV. Kim[8] has suggested that this is an indication of the onset of double excited states in N_2. Other explanations for this feature have also been advanced.[35,36] Because this shoulder is rather well reproduced when forming a Y plot from total photoabsorption cross section data or small-angle electron-energy-loss spectra[37] It would appear that it must be due to a structure in either the $X\,^2\Sigma_g^+$ or $A\,^2\Pi_u$ channel. This observation is not necessarily at odds with Kim's suggestion since shake-off contributions can occur in any partial ionization channel.

Many mechanisms have been suggested for the occurrence of the observed features. A shape resonance at a photon energy of 28 eV (Ref. 38) could be responsible for the feature observed at 12.7 eV. It has been suggested that the three features at 8.7, 7.1, and 4.8 eV are due to autoionization from Rydberg states,[8,39] converging to the $C\,^2\Sigma_u^+$ state of N_2^+, to the $X\,^2\Sigma_g^+$, $A\,^2\Pi_u$ and $B\,^2\Sigma_u^+$ states of N_2^+.[8] The small feature at 3.4 eV may be due to a shape resonance discovered in the theoretical calculations of Hermann[40] ($\sim$3-eV FWHM) in the ionization channel leading to the formation of the $(2\pi_u)^{-1}A\,^2\Pi_u$ state at 20 eV of photon energy. Finally we would like to suggest that the feature at 2.3 eV may be due to autoionization from a Rydberg state with an effective principle quantum number $n^*=3.92$, converging to the $B\,^2\Sigma_u^+$ state on N_2^+ which decays to the $X\,^2\Sigma_g^+$ ($v=0$) ground state of N_2^+. Note that this appears to the first observation of this feature in secondary electron spectra.

B. The region below 2 eV

Some autoionization features below 2 eV are observed in every spectrum, notably the one at 1.6 eV. For a possible analysis of these features we recorded the spectra down to ~ 0.4 eV of ejected energy at 60° and 90° of ejection angle using 2000-eV electrons. The spectra were converted to DDCS and were divided by the Rutherford cross section, $d\sigma_R/dE$ [see Eq. (4)]. The resultant quantity, $Z(T,W,\theta)$ is plotted on a linear W scale from 0.4 to 1.8 eV in Fig. 10 for $\theta=60°$. Assignments of these features are indicated by line numbers and the key to the line numbers is given in Table VIII.

The first five electronic states of N_2^+ are the $X\,^2\Sigma_g^+$, $A\,^2\Pi_u$, $B\,^2\Sigma_u^+$, $D\,^2\Pi_g$, and $C\,^2\Sigma_u^+$ states, which have elec-

tronic energies 15.58, 16.9, 18.73, 22.05, and 23.58 eV, respectively[18] above the ground state of N_2. There are Rydberg states converging to each of these electronic states of N_2^+. Any of these Rydberg states having energy greater than the energy of the ground state of N_2^+ can lead to autoionization.

The observed Rydberg states converging to the $A\,^2\Pi_u$ state, called the Worley series, with energies above 15.58 eV are shown in Table VIII. Similarly there is another series of Rydberg states converging to the $B\,^2\Sigma_u^+$ state of N_2^+ called the Hopfield series. Other possible autoionizing states are summarized in Table VIII.

V. CONCLUSIONS

In this paper we have presented the relative measurements of the DDCS for 200, 500, 1000, and 2000 eV primary electrons which are placed on an absolute scale by normalizing the elastic intensity at selected angles to absolute measurements. The elastic differential cross sections at 200, 500, 1000, and 2000 eV in the angular range of 30° to 150° are also presented.

The DDCS were fitted to a Legendre polynomial expansion and from the zeroth-order coefficient the $d\sigma/dW$ were evaluated. For convenience in using the data presented here the coefficients of the polynomial expansion for a few ejected energies and all the primary energies are presented in Table IX.

The photons resulting from the collisions of electrons with molecular nitrogen are found to be isotropically distributed as in the case of helium.[1] This result served as a check on the relative intensity scale determination.

The present experiment at 200-eV primary energy is in disagreement with the results of Shyn[11] at ejection angles below $\sim 80°$. The forward peak in his DDCS in this angular range is not present in our experiment. DuBois and Rudd's[4] experiment using 500-eV primary electrons is in good agreement with the present results except at lower ejected energies (< 10 eV). There are significant differences between the present angular distributions and those by OBP (Ref. 3) at all primary energies. However, at 1000- and 2000-eV primary energy the agreement is better than for the lower energies. If the agreement between our results for He and the more recent results by Erhardt

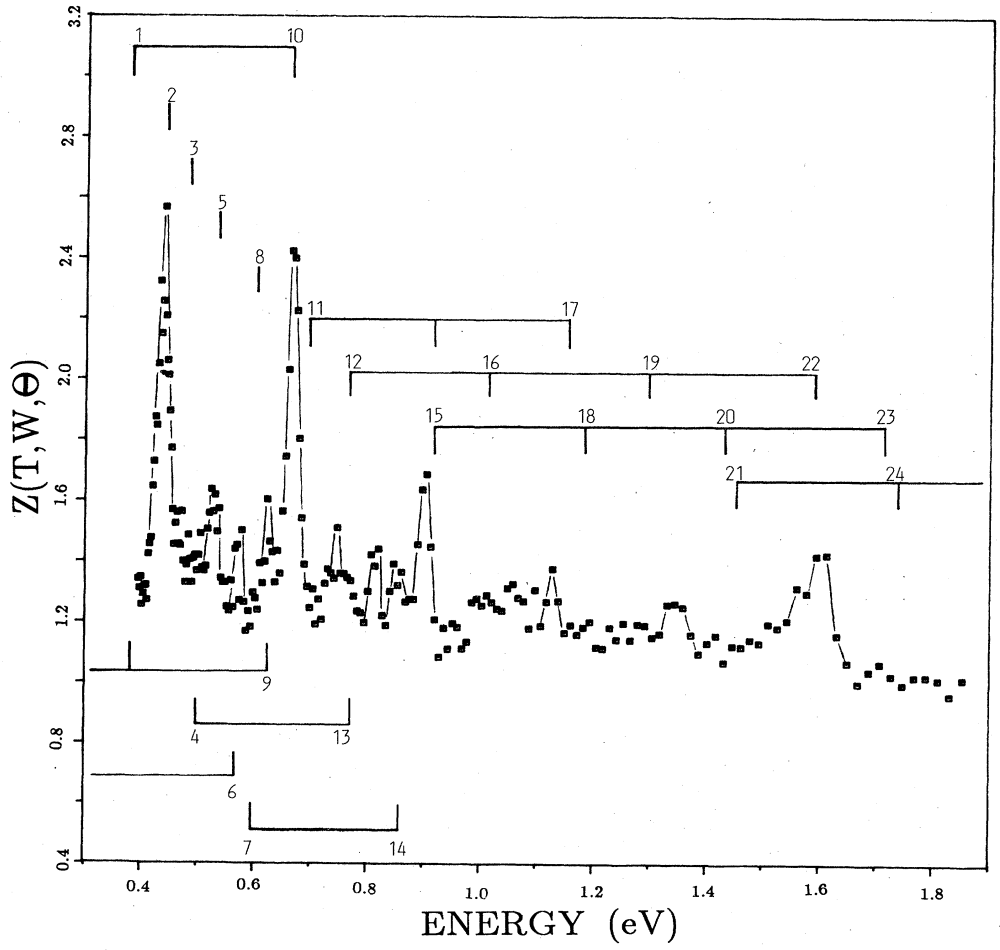

FIG. 10. A plot of the relative intensity $Z(T,W,\theta)$ as a function of the ejected energy W in the range from 0.4 to 1.8 eV. For a definition of Z see Sec. IV B. The primary energy was 2000 eV and the scattering angle was 60°.

et al.[45] is regarded as a calibration of our technique then we must regard the disagreement between our results and earlier measurements for N_2 as an indication of problems in the earlier works.

The experimental energy distributions of the ejected electrons are presented as a Platzman plot. Previously known shape resonances in photoelectron spectroscopy and photoabsorption are observed. In addition, features due to autoionization are observed. It appears that this is the first time that the autoionization feature at 2.3 eV has been observed in experiments measuring secondary electron cross sections. A possible explanation for the origin

TABLE VIII. A summary of the possible and observed autoionization lines in N_2 with ejected energies in the range ~0.4—2.5 eV. The number in the square brackets is the energy in eV of the state above the ground-state energy of N_2.

Autoionizing state	Orbital[a]	Comment	Ion final state	Ejected energy (eV)	Line no.
$O_5\ ^3\Pi_u$ ($v'=0$) [16.12]	$6s\sigma_g$	b	$X\ ^2\Sigma_g^+$ ($v=0$) [15.58]	0.52	5
$o_6\ ^1\Pi_u$ ($v'=0$) [16.15]	$6s\sigma_u$	b	$X\ ^2\Sigma_g^+$ ($v=0$)	0.57	6
			($v=1$)	0.30	
$o_4\ ^1\Pi_u$ ($v'=1$) [16.07]	$5s\sigma_g$	c	$X\ ^2\Sigma_g^+$ ($v=0$)	0.49	3
NP1 ($v'=1$) [16.21]		c	$X\ ^2\Sigma_g^+$ ($v=0$)	0.63	9
$O_4\ ^3\Pi_u$ ($v'=2$) [16.24]		c	$X\ ^2\Sigma_g^+$ ($v=0$)	0.66	10
			($v=1$)	0.39	1
$O_5\ ^3\Pi_u$ ($v'=1$) [16.35]	$6s\sigma_g$	c	$X\ ^2\Sigma_g^+$ ($v=0$)	0.77	13
			($v=1$)	0.50	4
NP1 ($v'=2$) [16.43]		c	$X\ ^2\Sigma_g^+$ ($v=0$)	0.86	14
			($v=1$)	0.59	7
$^1\Sigma_u^+$ ($v'=0$) [17.15]	$4s\sigma_g$	d	$X\ ^2\Sigma_g^+$ ($v=0$)	1.57	22
			($v=1$)	1.30	19
			($v=2$)	1.03	16
			($v=3$)	0.76	12
			$A\ ^2\Pi_u$ ($v=0$)	0.45	2
$^1\Sigma_u^+$ ($v'=0$) [17.31]	$\sigma_g(4s+4d)$	e	$X\ ^2\Sigma_g^+$ ($v=0$)	1.73	23
			($v=1$)	1.46	20
			($v=2$)	1.19	18
			($v=3$)	0.92	15
			$A\ ^2\Pi_u$ ($v=0$)	0.61	8
$^1\Sigma_u^+$ ($v'=0$) [17.86]	$5s\sigma_g$	f	$X\ ^2\Sigma_g^+$ ($v=0$)	2.28	26
			($v=1$)	2.01	25
			($v=2$)	1.74	24
			($v=3$)	1.47	21
			$A\ ^2\Pi_u$ ($v=0$)	1.16	17
			($v=1$)	0.92	15
			($v=3$)	0.68	11

[a]The designation of the Rydberg orbital is in the united-atom model as in Ref. 41. The rest of the electronic configuration is that for the ionic state to which the state is converging.

[b]This is a member of the Worley series converging to the $A\ ^2\Pi_u$ state of N_2^+ (16.70 eV).

[c]These are the states observed in Ref. 42 by Berkowitz and Chupka. Note that the larger internuclear separation for this state would only favor excitations to $v'>0$. It is therefore expected that the lines referred to by comment *b* are weak. NP1 stands for the first new progression reported by Ogawa (Ref. 43).

[d]A member of Hopfield's Rydberg series converging to the $B\ ^2\Sigma_u^+$ state of N_2^+ (18.75 eV).

[e]This is also a Rydberg state converging to the $B\ ^2\Sigma_u^+$ state of N_2^+. Here the orbital is described in the separated atom model.

[f]This state is the next member of Hopfield's Rydberg series mentioned in footnote c. This state is not given in Table 4 of Ref. 41 but it has been observed (Ref. 44).

of this peak has been presented.

The total ionization cross sections are derived from the present data by use of the Platzman plot and are in excellent agreement with those in Ref. 24. Empirical formulas were used to extrapolate the Y function of the Platzman plot to the high- and low-energy limits where necessary.

An analysis of the observed autoionization lines below 2.0 eV is presented. The agreement between the experiment and the line assignments points to the fact that the energy scale in the present experiment is accurate.

Finally we wish to point out that Platzman plots at high incident energies (1—3 keV) can be used to study

TABLE IX. Legendre polynomial fit coefficients, A_n, for selected ejected electron energies, W, and at different primary energies, T, in units of 10^{-20} cm^2 sr^{-1}. Both W and T are given in eV. See Eq. (2) in the text for details. The number in square brackets denotes the power of 10 by which the number is to be multiplied.

W (eV)	A_n (10^{-20} cm^{2}sr^{-1}) A_0	A_1	A_2	A_3	A_4	A_5
T=200 eV						
2.0	1.08[2]	−2.32[1]	−1.51[1]	−7.95	7.50[−1]	
4.0	9.03[1]	−4.13	−3.80	−1.81	6.08	
6.0	8.15[1]	3.55[−1]	−4.57	1.44[−1]	5.08	
8.0	7.04[1]	3.22	−3.29	−2.89	4.83	
10.0	6.14[1]	3.02	−4.57	−4.20	3.83	
15.9	4.04[1]	5.09	−3.76	−4.66	2.24	
20.0	2.77[1]	4.39	−3.24	−4.98	1.06	
40.0	8.87	2.94	−1.98[−1]	−3.18	−1.27	1.21[−1]
50.0	6.09	2.48	7.88[−1]	−2.19	−1.26	-2.88[−1]
T=500 eV						
2.0	4.93[1]	−1.95[1]	−6.56	3.82	4.99	
4.0	4.62[1]	−3.03	−4.60	5.30[−1]	2.71	
6.0	4.50[1]	1.34	−4.64	2.85[−2]	3.36	
8.0	4.03[1]	2.96	−4.75	−1.10	2.83	
10.0	3.57[1]	4.34	−4.84	−1.50	1.71	
15.9	2.49[1]	4.29	−4.46	−2.60	1.66	
20.0	1.73[1]	3.67	−3.99	−2.93	1.00	
40.0	5.57	2.11	−1.86	−1.97	7.97[−2]	9.80[−1]
50.0	3.57	1.57	−1.28	−1.55	−2.78[−1]	9.02[−1]
T=1000 eV						
2.0	3.76[1]	−1.03	−4.70	1.97	2.77	
4.0	3.06[1]	3.32[−1]	−3.84	1.67[−1]	1.19	
6.0	2.82[1]	1.01	−4.43	3.88[−1]	1.28	
8.0	2.46[1]	1.47	−4.74	−1.46[−1]	1.67	
10.0	2.20[1]	1.63	−4.73	−3.49[−1]	1.56	
15.9	1.52[1]	1.76	−3.83	−7.37[−1]	1.37	
20.0	1.03[1]	1.53	−3.19	−1.11	1.23	
40.0	3.33	8.81[−1]	−1.57	−8.38[−1]	5.37[−1]	5.05[−1]
50.0	2.13	6.69[−1]	−1.06	−7.23[−1]	3.54[−1]	5.01[−1]
T=2000 eV						
2.0	2.09[1]	1.14	−2.49	1.66[−1]	3.87[−1]	
4.0	1.73[1]	9.67[−1]	−3.82	−4.87[−1]	1.93[−2]	
6.0	1.61[1]	1.09	−3.92	−3.94[−1]	−3.27[−1]	
8.0	1.43[1]	1.07	−4.05	−4.49[−1]	−2.21[−1]	
10.0	1.28[1]	1.11	−3.94	−5.77[−1]	−2.06[−1]	
15.9	9.03	8.96[−1]	−3.25	−6.47[−1]	1.01[−1]	
20.0	6.15	7.66[−1]	−2.63	−5.93[−1]	1.65[−1]	1.03[−1]
40.0	1.97	4.06[−1]	−1.21	−4.39[−1]	3.14[−1]	2.14[−1]
50.0	1.27	2.84[−1]	−8.38[−1]	−3.42[−1]	2.90[−1]	2.33[−1]

shape resonances and autoionization structure in the ionization process. Models used to explain the origin of shape resonances and to make assignments in photo electron spectroscopy will now have to explain detailed information of the type presented here. Note that the demonstrated energy resolution is less than 8 meV below 1 eV. One possible extension of the present work is to use low incident electron energy to observe optically forbidden transitions in the ejected electron (pseudo photoelectron) spectrum.

All experimental data has been deposited with the Physics Auxiliary Service (PAPS).[46]

ACKNOWLEDGMENT

The authors wish to acknowledge support by the National Science Foundation under Grant No. CHE-83-09934.

[1]R. R. Goruganthu and R. A. Bonham, Phys. Rev. A **34**, 103 (1986).
[2]C. B. O. Mohr and F. H. Nicoll, Proc. R. Soc. London, Ser. A **144**, 596 (1934).
[3]C. B. Opal, E. C. Beaty, and W. K. Peterson, At. Data **4**, 209 (1972).
[4]R. D. DuBois and M. E. Rudd, Phys. Rev. A **17**, 843 (1978).
[5]A similar problem, with helium as the target gas, was examined in M. E. Rudd and R. D. DuBois, Phys. Rev. A **16**, 26 (1977).
[6]N. Oda, Radiat. Res. **64**, 80 (1975).
[7]N. Oda, F. Nishimura, and T. Ossawa, in *Electron-Molecule Collisions and Photoabsorption Processes,* edited by V. McKoy, H. Suzuki, K. Takayanagi, and S. Trajmar (Verlag Chemie International, Deerfield Beach, Florida, 1983), p. 33.
[8]Y. K. Kim, Radiat. Res. **61**, 21 (1975).
[9]Y. K. Kim, Radiat. Res. **64**, 96; **64**, 205 (1975).
[10]H. C. Tuckwell and Y. K. Kim, J. Chem. Phys. **64**, 333 (1976); Y. K. Kim, in *Proceedings of the Ninth International Conference on the Physics of Electronic and Atomic Collisions, Seattle, 1975* (University of Washington, Seattle, 1975), p. 741.
[11]T. W. Shyn, Phys. Rev. A **27**, 2388 (1983).
[12]T. W. Shyn and W. E. Sharp, Phys. Rev. A **19**, 557 (1979).
[13]M. Inokuti, in Radiological and Environmental Research Division Annual Report No. ANL-77-65, Argonne National Laboratory, 1977 (unpublished). Y. Hatano, in Argonne National Laboratory Report No. ANL-84-28, 1984 (unpublished). A good exposition of the various uses for these cross sections are given in the first nine articles in this report.
[14]R. R. Goruganthu and W. G. Wilson, Rev. Sci. Instrum. **55**, 2030 (1984).
[15]R. E. Kennerly, Phys. Rev. A **21**, 1876 (1980).
[16]H. J. Blaauw, R. J. Wagenaar, D. H. Barends, and F. J. de Heer, J. Phys. B **13**, 359 (1980).
[17]M. Inokuti, Rev. Mod. Phys. **43**, 297 (1971).
[18]K. Siegbahn, C. Nordling, G. Johansson, J. Hedman, P. F. Hede'n, K. Hamrin, U. Gelius, T. Bergmark, L. O. Werme, R. Manne, and Y. Baer, *ESCA Applied to Free Molecules* (North-Holland, Amsterdam, 1969), p. 66.
[19]R. H. J. Jansen, F. J. de Heer, H. J. Luyken, B. Luyken, B. van Wingerden, and H. J. Blaauw, J. Phys. B **9**, 185 (1976).
[20]T. W. Shyn and G. R. Carignan, Phys. Rev. A **22**, 923 (1980).
[21]R. D. DuBois and M. E. Rudd, J. Phys. B **9**, 2657 (1976).
[22]D. Herrmann, K. Jost, J. Kessler, and M. Fink, J. Chem. Phys. **64**, 1 (1976).
[23]See p. 64 of Ref. 18.
[24]D. Rapp and P. Englander-Golden, J. Chem. Phys. **43**, 1464 (1965).
[25]J. P. Bromberg, J. Chem. Phys. **52**, 1243 (1970).
[26]J. Kambara and K. Kuchitsu, Jpn. J. Appl. Phys. **11**, 609 (1972).
[27]The IAM model for the elastic DCS for a homonuclear diatomic is given by

$$\frac{d\sigma}{d\Omega}=2|f|^2\left[1+\frac{\sin(KR)}{KR}\exp(-l^2K^2/2)\right].$$

Here, f is the atomic partial wave scattering amplitude, K is the momentum transferred to the target by the electron, R is the internuclear separation, and l^2 is the mean square amplitude of vibration in the molecule. For details see: R. A. Bonham and M. Fink, *High Energy Electron Scattering* (Van Nostrand Reinhold, New York, 1974), p. 108.
[28]M. Fink and J. Ingram, At. Data **4**, 129 (1972).
[29]In Ref. 7, p. 35, the first sentence under experimental results must be 1000-eV instead of 100-eV if the caption for Fig. 2 is correct, which appears to be the case.
[30]P. R. Woodruff and G. V. Marr, Proc. R. Soc. London, Ser. A **358**, 87 (1977).
[31]E. W. Plummer, T. Gustafsson, W. Gudat, and D. E. Eastman, Phys. Rev. A **15**, 2339 (1977).
[32]J. A. R. Samson, G. N. Haddad, and J. L. Gardner, J. Phys. B **10**, 1749 (1977).
[33]A. Hamnett, W. Stoll, and C. E. Brion, J. Electron Spectrosc. Relat. Phenom. **8**, 367 (1976).
[34]I. L. Dehmer, A. C. Parr, S. Wallace, and D. Dill, Phys. Rev. A **26**, 3283 (1982).
[35]H. D. Cohen and U. Fano, Phys. Rev. **150**, 30 (1966).
[36]H. C. Tuckwell, J. Phys. B **3**, 293 (1970).
[37]S. N. Ketkar (private communication).
[38]G. R. J. Williams and P. W. Langhoff, Chem. Phys. Lett. **78**, 21 (1981).
[30]K. Codling, Astrophys. J. **143**, 552 (1966).
[40]M. R. Hermann, Ph. D. thesis, Indiana University, 1984.
[41]A. Lofthus and J. Krupenie, J. Phys. Chem. Ref. Data **6**, 113 (1977).
[42]J. Berkowitz and W. A. Chupka, J. Chem. Phys. **51**, 2341 (1969).
[43]M. Ogawa, Can. J. Phys. **42**, 1087 (1964).
[44]E. Lindholm, Arkiv. Fys. **40**, 111 (1969).
[45]H. Erhardt, K. Jung, R. Muller-Fiedler, and P. Schlemmer, Argonne National Laboratory Report No. ANL-84-28, 1983 (unpublished).
[46]See AIP document No. PAPS PLRAA-35-0540-60 for 60 pages of the original experimental data. Order by PAPS number and journal reference from American Institute of Physics, Physics Auxiliary Publication Service, 335 East 45th Street, New York, NY 10017. The price is $1.50 for each microfiche (98 pages) or $5.00 for photocopies of up to 30 pages, and $0.15 for each additional page over 30 pages. Airmail additional. Make checks payable to the American Institute of Physics.